Asian Journal of Geological Research

3(4): 1-15, 2020; Article no.AJOGER.61526

Structures and Depth to Magnetic Source Assessment of Auchi Sheet 266, South-Eastern Nigeria

Mam D. Tawey[1*], Ibrahim A. Adesoji[1] and Ismail A. Garba[1]

[1]National Water Resources Institute, Mando Road, Kaduna, Nigeria.

Authors' contributions

This work was carried out in collaboration among all authors. Author MDT designed the study, performed the statistical analysis, wrote the protocol and wrote the first draft of the manuscript. Author IAA managed the analyses of the study. Author IAG managed the literature searches. All authors read and approved the final manuscript.

Article Information

Editor(s):
(1) Dr. Ahmed Abdelraheem Frghaly, Sohag University, Egypt.
Reviewers:
(1) Myriam Patricia Martinez, CONICET-National University of San Juan (UNSJ), Argentina.
(2) Ahmed Tarshan, Saint Petersburg State University, Russia.
Complete Peer review History: http://www.sdiarticle4.com/review-history/61526

Original Research Article

Received 01 August 2020
Accepted 05 October 2020
Published 21 October 2020

ABSTRACT

The current study was designed to provide a consistent and detailed understanding of the Structural disposition and magnetic source depth of Sheet 266, south-east Nigeria in the Auchi region by applying three source edge mapping techniques: horizontal gradient magnitude; tilt derivative and Euler deconvolution to aeromagnetic data obtained from Nigeria Geological Survey Agency Abuja (NGSA). To achieve the above objective, there was a need to correct the latitudinal effect on data obtained at low latitudes just as the present case, the total magnetic intensity (TMI) data was reduced to the pole (RTP) and regional magnetic anomalies were extracted from the RTP data to obtain the residual anomaly data using the upward continuation technique. To establish the boundaries of the magnetic sources, various source edge mapping techniques such as Analytic signal (AS), Horizontal Gradient Magnitude (HGM) and Tilt Derivative (TDR) were applied. A strong correlation between these techniques has been found, suggesting that their incorporation may contribute to delineating the structural mechanism of the study area. A comprehensive structural map based on the findings was therefore built. The key tectonic patterns in the study region are typically interpreted to predominantly ENE-WSW trend followed by WNW-ESE trend. In the study

**Corresponding author: Email: taweymam@gmail.com;*

area, depth to magnetic source estimation using 3D Euler deconvolution and source parameter imaging (SPI) has also shown that the two techniques complement each other with depth estimation and general depth to magnetic source was 50 m in the basement portion of the study area and >2000 m in sedimentary portion as seen from both SPI and 3D Euler deconvolution techniques.

Keywords: Source edge; auchi; RTP and deconvolution.

1. INTRODUCTION

The study area is situated between longitudes 6^0 E to 6^0 30^1 and latitudes 7^0 N to 7^0 30^1 N (Fig. 1) with an average area of 3, 025 km^2 and topography ranging from 14 m low to 662 m high (Fig. 2) and form part of south-western Nigerian basement complex in the north and part of the Dahomey basin in the southern part of the study area (Fig. 3). The south-west Nigerian basement complex is tectonically part of the Pan-African mobile belt and is situated between the West Africa craton, Congo craton and south of the Tuareg shield [1]. The basement complex was deformed by numerous pre-Cambrian tectonic events which were followed by progressive regional metamorphism according to [2-6]. On the basement rocks, each of the tectonic events created characteristic imprints. The Pan-African case, however, was so widespread that much of the systems of the earlier events were wiped out, leaving only their traces. The structural patterns of both the planar and linear systems are along with the trends of N-S, NE-SW, NW-SE and occasionally E-W in Nigeria according to [7-10].

Several papers were published on the analysis of aeromagnetic data regarding geological structures/lineament delineation within the southwestern Nigerian basement complex [12-17] and all used magnetic data evaluation in different ways to delineate geological structures in parts of the southwestern Nigerian Precambrian Basement Complex. Situated in the West African Gulf of Guinea, the Benin (Dahomey) Basin runs parallel to the coastal shores of Ghana, Togo, the Republic of Benin and southwestern Nigeria. It is an extensive basin from southeastern Ghana across Togo and the Republic of Benin to southwestern Nigeria, where it is stratigraphically isolated from younger Niger Delta basin. The basin is made up of sedimentary Cretaceous-Tertiary sequences that outcrop roughly parallel to the ancient coastline in an arcuate belt. The Dahomey basin's Tertiary sediments thin out to the east and are partly cut off from the Niger Delta basin's sediments against the Okitipupa basement ridge. During the drifting phases of separation of South America and Africa in the Campanian to Tertiary, the evolution of the Dahomey basin is due to the transcurrent movements of the oceanic fracture systems, in particular the Romanche, Chain and Charcot fractures. As a consequence of continental drift, the division of the African and South American landmasses contributed to the eventual opening

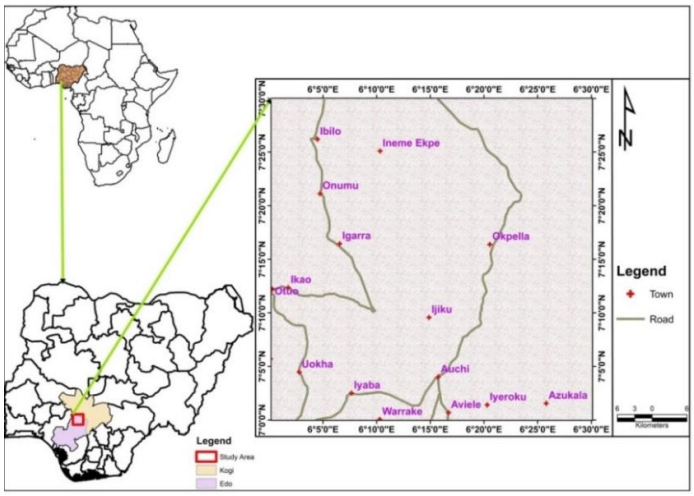

Fig. 1. Location map of the area

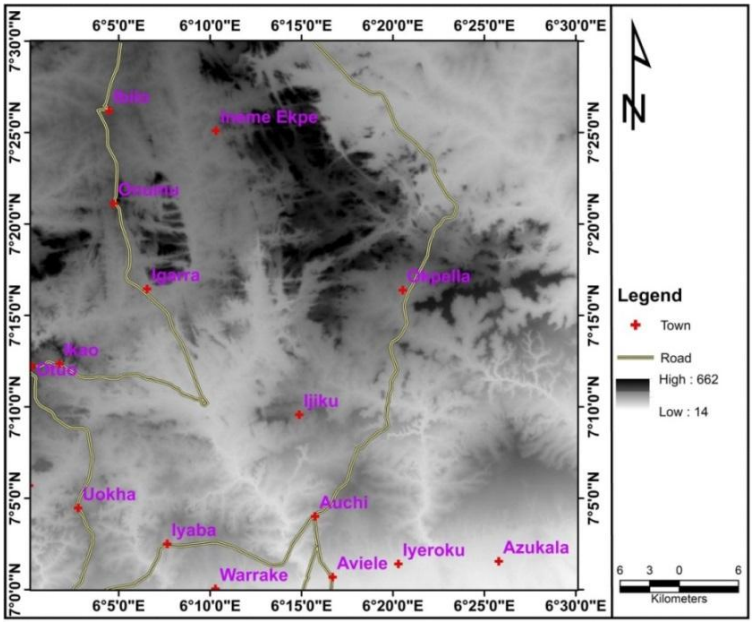

Fig. 2. SRTM Digital Elevation Model (DEM) inverted, showing topographical variation

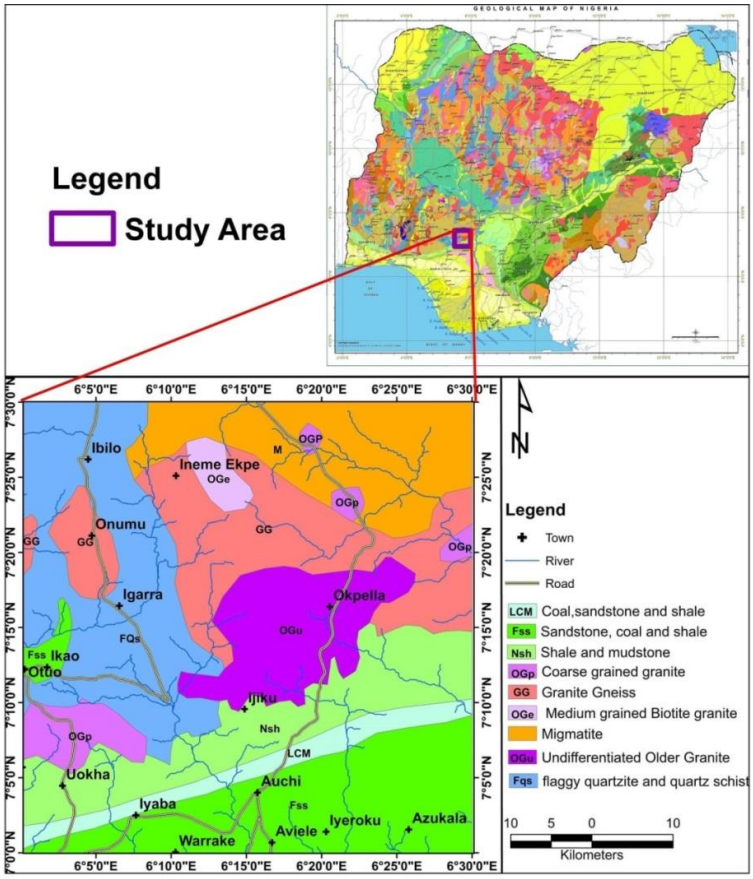

Fig. 3. Geologic map of the area [11]

of the Atlantic Ocean during the Mesozoic Era [18]. There have been many theories established as to the origin and/or evolution of the basin. However, based on several features characterizing the basin [19,20], the rift hypothesis is widely supported. The stratigraphy of the eastern Dahomey basin suggests that the basement complex of southwestern Nigeria is inconsistently overlapped by the Ise Formation. The formation consists of grits and conglomerates at the base and is overlain with intermediate kaolinite by coarse-grained loose sands. Neocomian to Albian is the age of the Ise Formation. The Afowo, Araromi, Ewekoro and Akinbo Formations are therefore stratigraphically succeeded this unit [19].

Previous studies in the study area have presented the Dahomey Basin as a low petroleum potential sedimentary basin [21]. It is presumed that the basin contains a deep sediment wedge, up to 3000 m, which thickens offshore [22]. Granite Gneiss, Undifferentiated Older Granite, Coarse-grained granite, Migmatite, Fine to Medium-grained Biotite granite, Flaggy quartzite and quartz schist, Sandstone, coal and shale, Shale and mudstone and Coal, sandstone and shale are the rock forms within the research area. The current study aims to delineate geological structure and depth to magnetic sources using different techniques of detection of source edges and depth estimation such as tilt derivative (TDR) as suggested by[23-26], analytical signal (AS) as suggested by[27], horizontal gradient magnitude (HGM) technique that can be used to map linear features such as fault zones and/or dykes from potential field data $[28-30]$, the Euler deconvolution used for depth, contacts and source geometry by [31,32] and source parameter imaging by [33-36] to determine the depth to the magnetic source.

2. MATERIAL AND METHODS

Auchi's aeromagnetic data (sheet 266) was collected from the Geological Survey Agency of Nigeria (NGSA). In 2009, the NGSA performed an aeromagnetic survey and collected data using a proton precession magnetometer with a resolution of 0.01 nT. The airborne geophysical work was performed by Fugro Airborne Surveys and the aeromagnetic surveys were flown at 500 m-line spacing and 80 m-terrain clearance with flight line direction in the direction of 135 azimuths while the direction of the tie line was 45 azimuths.

For equipment specifications, Magnetometers used were 3 x Scintrex CS3 Cesium Vapour Data Acquisition System was FASDAS and Magnetic Counter was also FASDAS. Radar Altimeter used was KING KR405/KING KR405B and Barometric Altimeter used was ENVIRO BARO/DIGIQUARTZ. For Navigation specifications, the Flight Path Tracking was Digital and Flight Path Navigation was Novatel 3151R/Omnistar RTDGPS. Flight Path Recovery was Digital and Flight Path Processing was performed using Real-Time Differential GPS and the Aircraft used for the survey were supplied by Fugro Airborne Surveys which included: Aircraft Cessna Caravan 208B ZS-FSA, Aircraft Cessna Caravan 208 ZS-MSJ and Aircraft Cessna 406 ZS-SSC. For plotting specifications, the projection method used was the universal transverse Mercator (UTM) with spheroid-Clarke 1880 (modified) at central meridian 33 degrees east and central scaling factor 0.9996 and datum arc 1960. The x bias was 500 000 meters and y bias 0 meters with grid mesh size 50 meters. Usually, before gridding, many corrections needed to be applied to magnetic data, i.e. heading, lag and diurnal correction and all have been applied to the aeromagnetic data by Fugro surveys. The magnetic data acquisition and airborne surveys data processing were done completely by Fugro airborne surveys.

Software such as Oasis Montaj version 10.3, Arc Map version 10.5 and Rockwork version 2016 was used to generate the maps used by the authors in this study. First, the total magnetic intensity data (Fig. 4) was reduced to the magnetic pole and overlaid with the area's geology. This was appropriate for the anomaly to be centered directly above its respective causative source [37-41] and was accomplished using -10.62^0 inclination and -2.76^0 declination of the centre point of the study area using (2005 IGRF). Since the RTP often introduces noise during aeromagnetic data interpretation, especially for data collected very close to the equator as well as the current study area, stable reduction to the pole method was used to avoid this effect by applying -90^0 amplitude correction inclination, producing a balanced RTP map (Fig . 5). After pole reduction, it is important to enhance the data signal by separating the short wavelengths (local or residual) and long wavelengths (regional) components of the total field anomaly data. The former are shallow magnetic anomalies (i.e., near-surface sources), while the latter are the sources of deep-seated magnetic anomalies. This was accomplished by

employing an upward continuation filter. The upward continuation filter's frequency response is given as

$$F_u\,(u,v,h) = e^{-2\pi h}(u^2 + v^2)^{\frac{1}{2}} \quad (1)$$

Where h is the height at which the field is continued and in the frequency domain, "u" and "v" are equal to x and y coordinates. When deeper sources magnetic fields are subtracted from the total field, the shallow magnetic field intensity known as the residual field is the result[42,43]. At a depth of 30 km, the RTP data was upward continued representing the area's regional grid and this was subtracted from the RTP grid to obtain the residual grid view as an image (Fig. 6). This is represented mathematically in equation 2.

RESIDUAL grid-REGIONAL grid 2 = RTP grid (2)

The analytic signal (AS) technique was applied to the areas TMI data and is defined as the square root of the sum of the squares of vertical derivative (dz) and the two horizontal derivatives (dx and dy) of the total magnetic field ΔT [27]. The AS peaks are directly correlated with and symmetrically oriented over their magnetic causative bodies i.e, the AS is independent of the inclination of the magnetic field. This avoids the difficulties that are often encountered when the direction of magnetization of the causative bodies is not established in the traditional reduction method to pole for ΔT. Besides, the AS has similar features to the derivative characteristics of the magnetic field, such that it is very sensitive to edge effects of the causative magnetic bodies as display on Fig. 7 [27], showed that the amplitude of the analytic signal can be calculated using the following expression from the three orthogonal gradients of the total magnetic field:

$$|A(X,Y)| = \sqrt{\left(\frac{\delta T}{\delta x}\right)^2 + \left(\frac{\partial T}{\partial y}\right)^2 + \left(\frac{\delta T}{\delta z}\right)^2} \quad (3)$$

Where A(x, y) is the amplitude of the analytic signal at (x, y) and T is the observed magnetic anomaly at (x, y).

The magnetic field's horizontal gradient (Fig. 8) in a given direction improves the magnetic field's lateral variations and attenuates its regional trend in that direction [44]. In places where the magnetic susceptibility contrast is higher, the derivative can achieve a maximum/minimum, thereby illustrating discontinuities perpendicular to the derivation direction and more clearly distinguishing the faults and structural edges as in (Fig. 8). In other words, the horizontal gradient method is the easiest way to estimate the bodies' contact positions at depths. The significant advantage of the horizontal gradient method is its low sensitivity to noise in the data since it requires only the measurement of the two horizontal field derivatives of the first order [45]. If M is the magnetic field, then the magnitude of the horizontal gradient (HGM) is given by.

$$HGM\,(x, y) = \sqrt{\left(\frac{\partial M}{\partial x}\right)^2 + \left(\frac{\partial M}{\partial y}\right)^2} \quad (4)$$

Under the following assumptions, this feature gives a peak anomaly above magnetic contacts [45]: (1) the regional magnetic field is vertical, (2) the magnetizations are vertical, (3) the contacts are vertical, (4) the contacts are discrete, and (5) the sources are dense. Violations of the first four assumptions which cause the peaks to move away from the contacts. Violations of the fifth assumption will lead to secondary peaks which will be parallel to the contacts.

[25] showed that the zero value of the TDR-filtered Total Magnetic Intensity (TMI) data (Fig. 9) locates the edges of the sources of the TMI anomaly and has the advantage of equalizing the amplitudes of potential field anomalies for short and long wavelengths. The TDR was first described by [26] before being further refined by[25] as:

$$\theta = \tan^{-1}\left[\frac{\partial T}{\partial z}\Big/\frac{\partial T}{\partial h}\right] \quad (5)$$

Where

$$\frac{\partial T}{\partial h} = \sqrt{\left(\frac{\partial T}{\partial x}\right)^2 + \left(\frac{\partial T}{\partial y}\right)^2} \quad (6)$$

$\frac{\partial T}{\partial x}, \frac{\partial T}{\partial y}\ and \frac{\partial T}{\partial z}$ in the equations are first-order derivatives of the magnetic field in the x, y and z directions. A new technique (the tilt-depth method) was recently introduced that locates vertical contacts and the depth of a magnetized body from RTP magnetic data [46]. The spatial position of the magnetic source edges is delineated by the zero contours of TDR, while the depth to the source is the distance between zero and either -45 ° or +45 ° contour or their average.

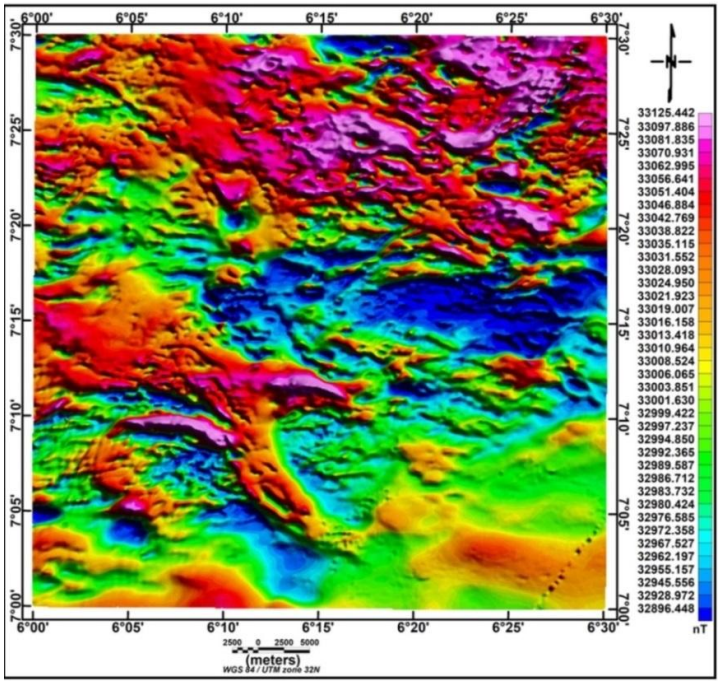

Fig. 4. Total magnetic intensity map (TMI)

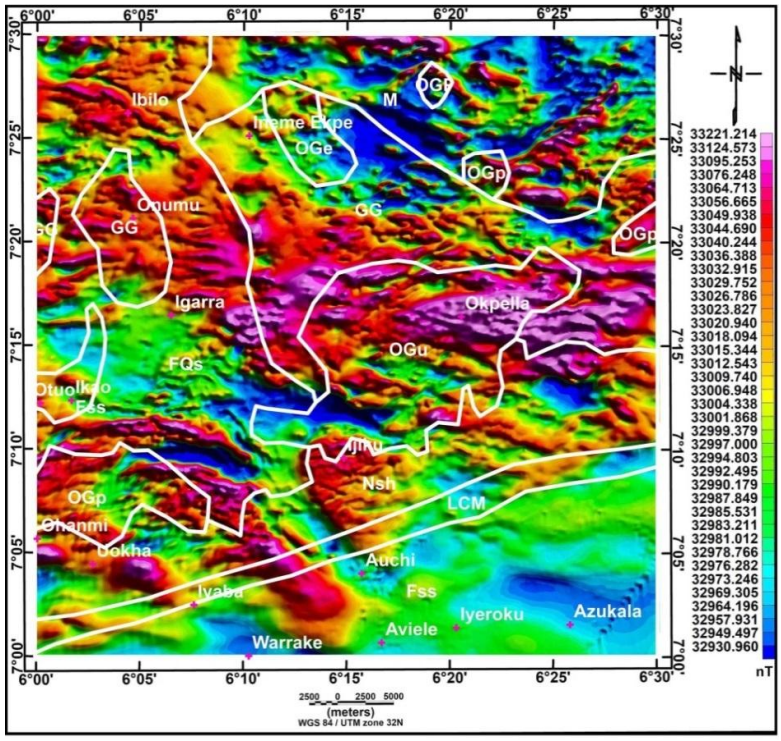

Fig. 5. Total magnetic intensity map Reduced to Pole (RTP) with Geology of the area

Granite Gneiss = GG, Undifferentiated Older Granite = OGu, Coarse-grained granite = OGp, Migmatite = M, Medium fine to medium-grained Biotite granite = OGe, Flaggy quartzite and quartz schist = FQs, Sandstone, coal and shale = Fss, Shale and mudstone and Coa =Nsh, sandstone and shale = LCM

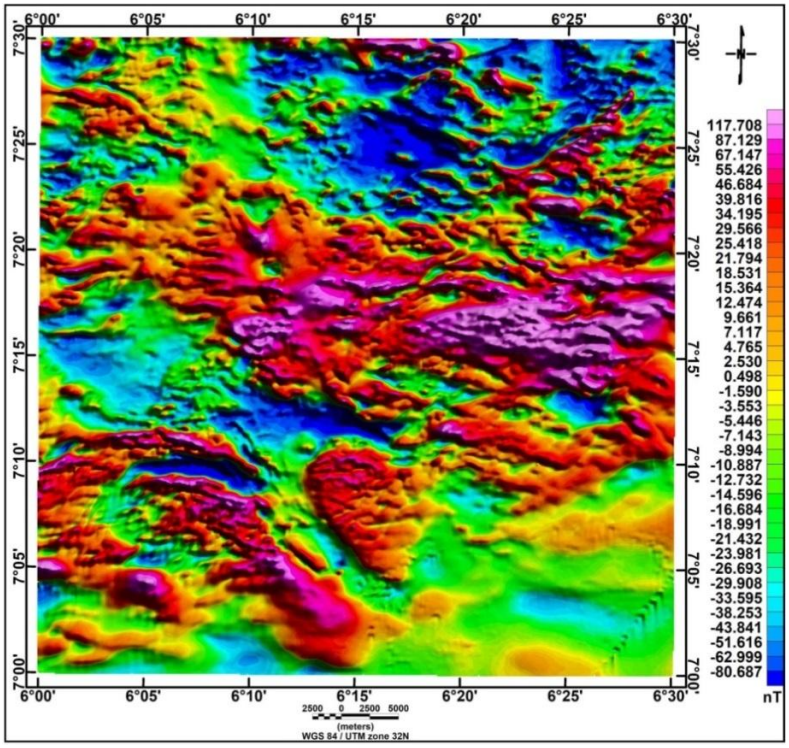

Fig. 6. Residual magnetic intensity map (RMI)

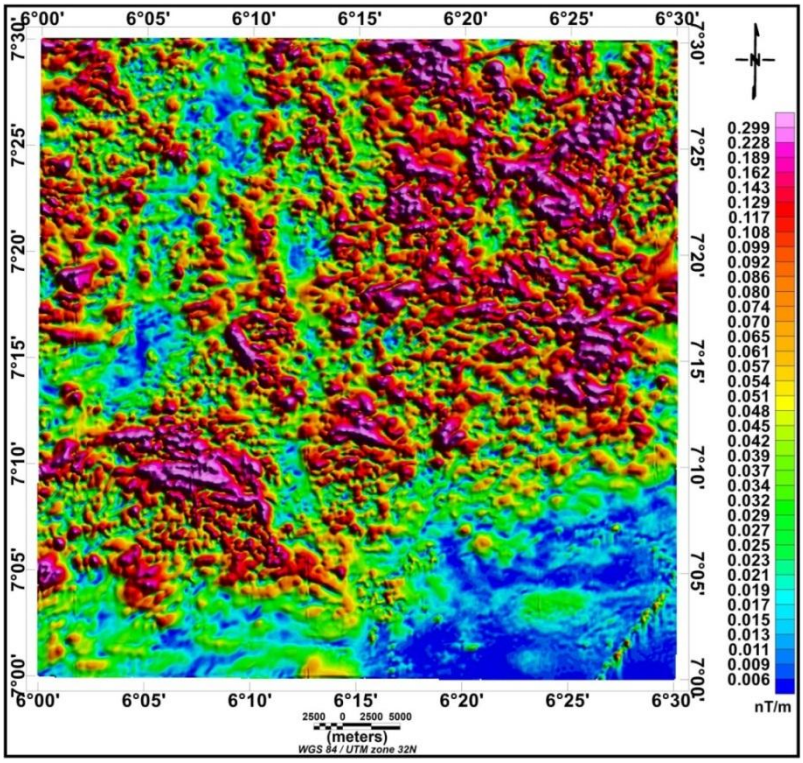

Fig. 7. Analytic Signal Map (AS)

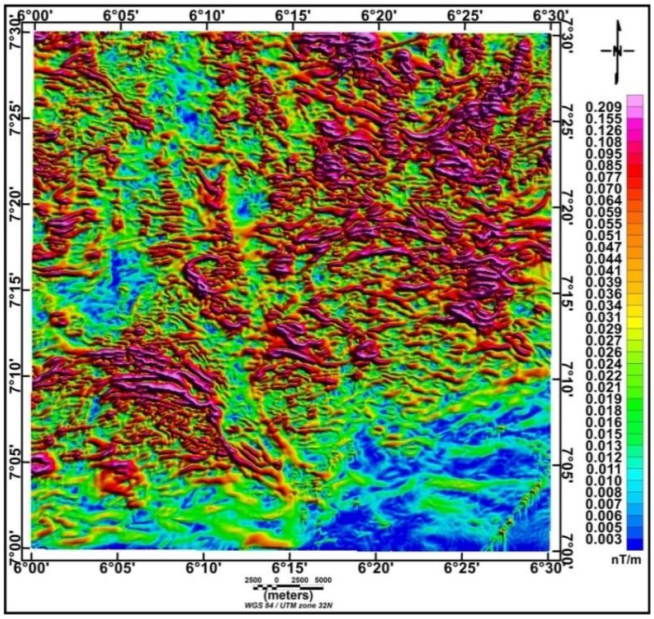

Fig. 8. Horizontal Gradient Magnitude (HGM)

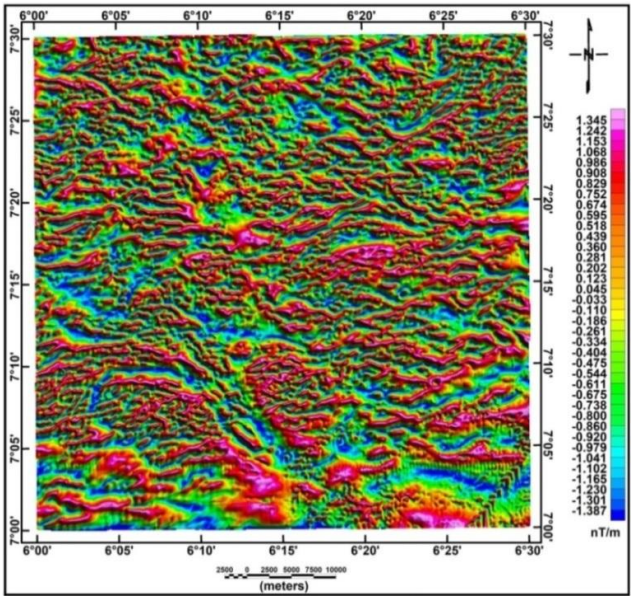

Fig. 9. Tilt Derivative (TDR)

The standard Euler deconvolution utilizes three orthogonal gradients of any possible potential field quantity to calculate the position of a source body. According to [8], It is possible to describe the 3D form of Euler's equation as:

$$(x - x_0)\frac{\delta T}{\delta x} + (y - y_0)\frac{\delta T}{\delta y} + (z - z_0)\frac{\delta T}{\delta z} = N(B - T) \quad (7)$$

Where the coordinates of a magnetic source are $x_0, y_0, and\ z_0$, $\frac{\partial T}{\partial x}, \frac{\partial T}{\partial y}\ and\ \frac{\partial T}{\partial z}$ are the derivatives of the total field versus x, y and z, respectively, N represents the structural index (SI) and relates to the rate of change of a potential field with the distance. In the overestimated scheme of linear equations, the location and depth of the sources are solved for each location of the moving window [31,32]. B is a local context inside a

sliding window with an adjustable size reflecting the "regional" area. The SI is based on the geometry of the source and its range for magnetic sources is between 0 to 3 and 0 to 2 for gravity sources. [47] showed that the SI relies on the type and physical parameters of the potential field, providing an outstanding description of the characteristics of the homogeneity equation of Euler in general and of the SI in particular. Structural indexes (SI= 0, 1 , 2 and 3) have been used in this work (Figs. 10a, 10b, 10c and 10d).

To determine the depth of the magnetic source within the study area, the source parameter imaging (SPI) as generated by [34-36] was used (Fig. 11). Often, the technique is referred to as the local wavenumber process. The maximum local wavenumber is located over isolated contacts and depths can be measured without the thickness of source bodies being assumed [48].

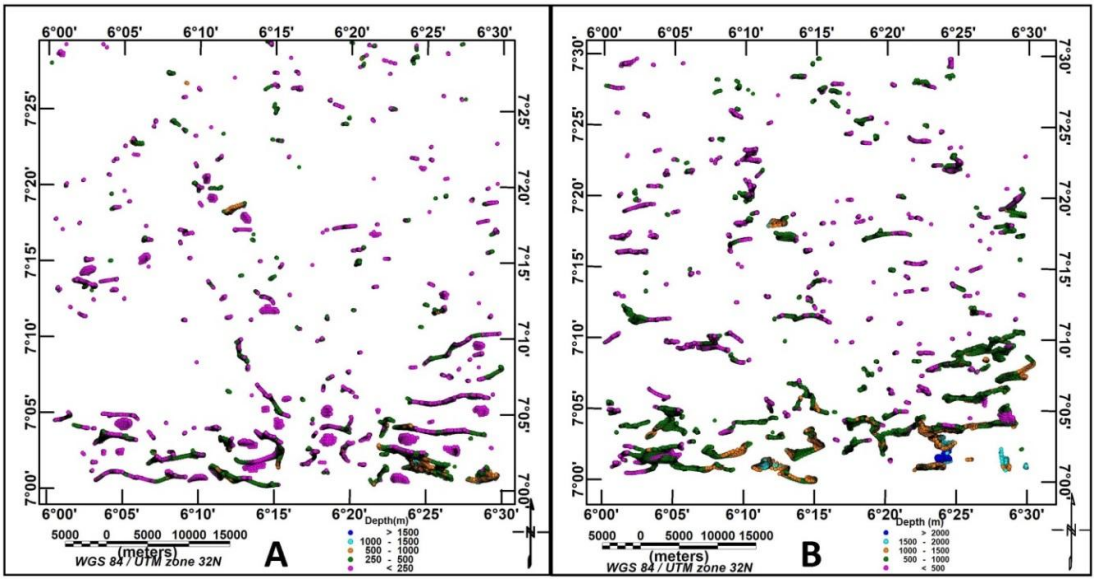

Fig. 10 a. Euler solutions structural index (SI=0) and b. Euler solutions structural index (SI=1)

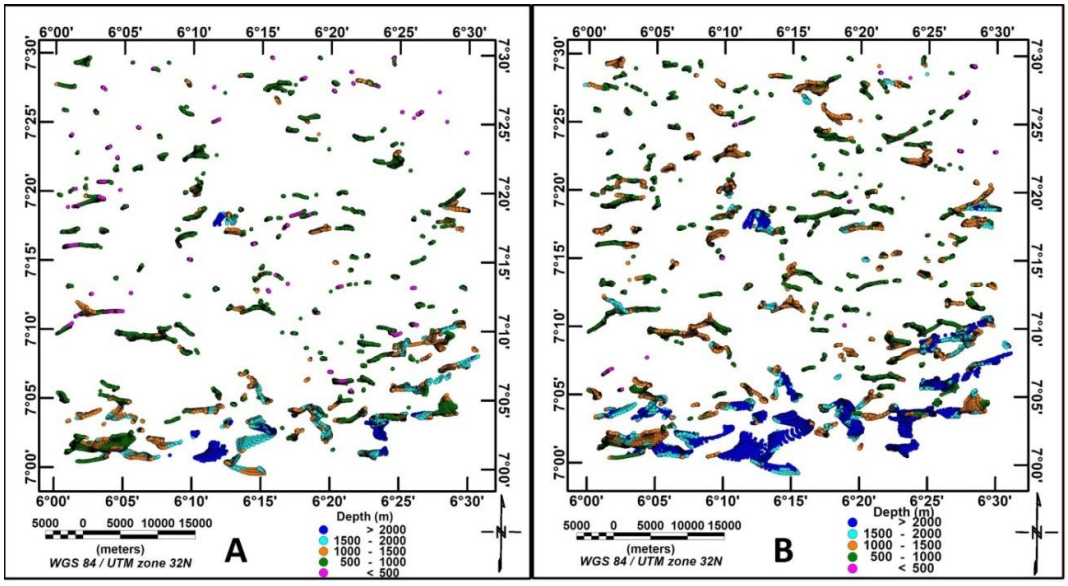

Fig. 10 c. Euler solutions structural index (SI=2) and d. Euler solutions structural index (SI=3)

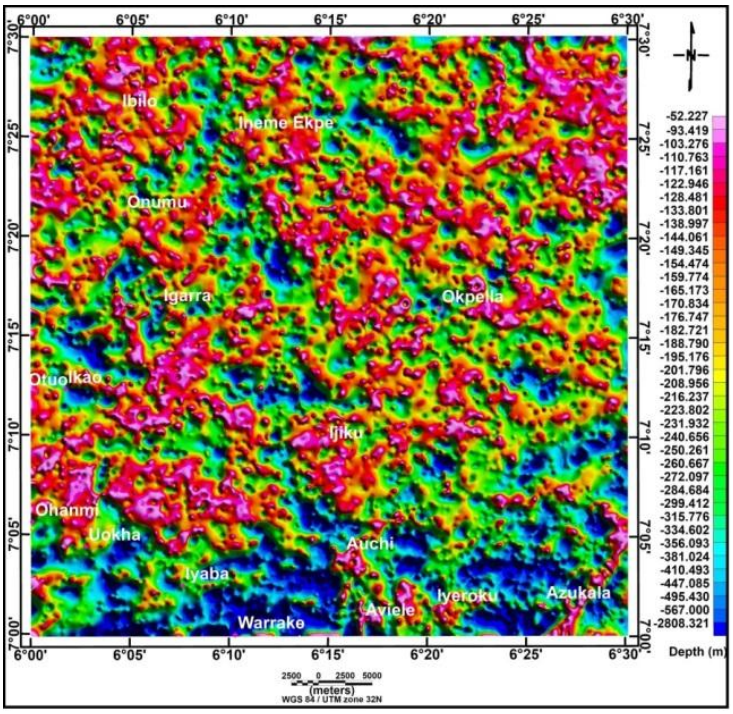

Fig. 11. Depth variation across the study area (SPI Map)

SPI is a technique that is good in determining magnetic depths based on the extension of complex AS; it is also called the local wavenumber. The original SPI approach works for two models which are: a 2-D sloping touch or a thin-sheet dipping 2-D. The local wavenumber is defined for the magnetic field f, by equation 8:

$$k = \frac{\frac{\partial^2 f \partial f}{\partial x \partial z \partial x} - \frac{\partial^2 f \partial f}{\partial x^2 \partial z}}{\left(\frac{\partial f}{\partial x}\right)^2 + \left(\frac{\partial f}{\partial z}\right)^2} \quad (8)$$

The maxima of k are located directly over the isolated contact edges for dipping contact and are independent of magnetic inclination, declination, dip, strike and any remnant magnetization. At the source edge, the depth is determined from the reciprocal of the local wavenumber i.e

$$Depth_{x=0} = \frac{1}{k_{max}} \quad (9)$$

3. RESULTS AND DISCUSSION

Fig. 4 reflects the map of the study area's total magnetic intensity (TMI). From the diagram, the regions with high magnetic intensity are areas with low magnetic intensity and the regions with low magnetic intensity are areas with high magnetic intensity. This misrepresentation is referred to as directional noise found in areas of low magnetic latitude due to the inclination of the magnetic field of the Earth at this low latitude, and this issue has been resolved by reducing the overall magnetic intensity to the pole where the magnetic field of the Earth is vertical (Fig. 5) overlaid with the area's geology. Magnetic intensities range from a minimum of 32930.960 nT to a maximum of 33221.214 nT from the RTP map, and magnetic highs are observed around Okpella and north to west of Igarra. The high magnetic intensity here is associated with a basic magmatic intrusion. The sedimentary rocks occupy the southern part of the map with low magnetic intensity, just as the geology of the region is divided into two, where the basement rocks occupy the northern portion of the map with high magnetic intensity values. The dyke-like feature cutting through the sedimentary portion of the map around the north of Warrake could be a magmatic intrusion of basaltic composition. Fig. 6 is the local magnetic intensity map of the area otherwise referred to as the residual magnetic intensity. The RMI value here ranges from a minimum of -80.687 nT to a maximum of 117.708 nT. A complex occurrence of magnetic highs and lows in the northern portion of the map may be due to the presence of deep-seated structures. Fig. 7 is the region's analytic signal (AS) map and can be used to

delineate the basement and the sedimentary portion of the study area. The northern part of the map is defined by high amplitude of range 0.099-0.299 nT / m unique to the basement; this can be correlated with the geology of the region (Fig. 3), while the southern part of the map is characterized by low analytic signal amplitude values ranging from 0.006 nT / m to 0.092 nT / m. The map also shows discontinuities that occupy the basement portion of the study area.

The HGM map (Fig. 8), just like the AS map (Fig. 7), has identified the faults and edges of the structures that are prevalent within the basement part of the study area. To separate the basement and the sedimentary portion of the study area, the HGM map here can be used. The basement portion of the map (Fig. 8) has indicated the edges of the anomalies while in the sedimentary portion of the map, there is none (Fig. 8).

The map for TDR is depicted by Fig. 9 which has defined the edges of the anomaly and equalized the amplitudes within the studied area of both the short and long wavelength potential field anomaly.

For contacts and faults / structures, 10 a and b reflect Euler deconvolution with structural index (SI= 0 and1) [31]. From the diagram, based on the Euler solutions for contacts, the basement part of the diagram is distinguishable from the sedimentary section. Fewer Euler solutions are characterized by the basement part of the diagram, while more Euler solutions are characterized by the sedimentary section. System of Faults in Fig. 10 b has been categorized into five classes and faults that occur at a depth less than 500 m are the most prevalent, followed by faults that occur at a depth of 500 m to 1000 m. The deepest occurrence of faults here is more than 2000 m. Fig.10 c and d represent Euler solutions with structural index (SI= 2 and3) [31], for pipe / horizontal bodies and spherical bodies. In Fig. 10 c, the horizontal bodies and pipes occur at depths of 500 m-1000 m, followed by those that occur at depths of 1000 m-1500 m. Likewise, Fig 10 d, is Euler solutions with structural index (SI = 3) for spherical bodies, the spherical bodies are uniformly distributed here but occur mostly at depths between 500 m and 1500 m.

Fig. 11 revealed magnetic source depth ranging from 52.227 m for the northern part of the region specifically for the basement part to a depth of 2808.321 m for the sedimentary part in the southern part of the area coinciding with a depth greater than 2000 m delineated from the Euler solution.

3.1 Structures / Lineament Analysis

Using the HGM map, the maximum ridges were delineated over the edges of faults within the study region (Fig. 8). These structures delineated (Fig. 12 a) were statistically analyzed As shown in the rose diagram (Fig. 12 b) and this showed that the most predominant tectonic activity affecting the region is the ENE-WSW, followed by WNW-ESE trends as stated by [49], which evaluated structures within the basement complex of north-central Nigeria and concluded that the ENE-WSW is the most predominant

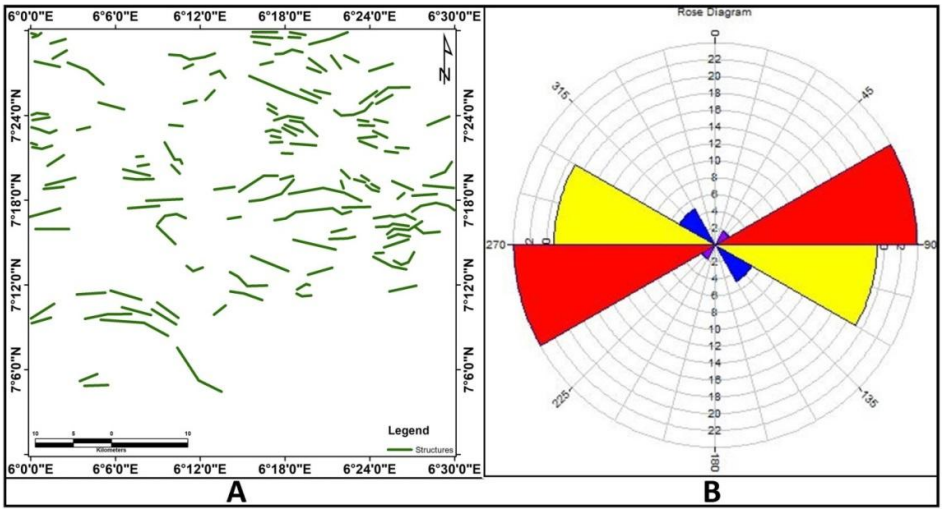

Fig. 12. a. Structural map of the area and b. Rose diagram of the structures

tectonic that has affected the Nigerian basement complex. The Euler solutions with SI = 1 was plotted on the delineated structures as shown in Fig. 13. This confirms the occurrence of these structures using the Euler solution map as previously described. The study area is dominated by most of the structures that occur at depth < 500 m, especially the northern part that is explicitly basement in nature. The Euler solutions with SI=1 were also plotted on the TDR map and these solutions were seen to align with the TDR map's edges and zero contours (Fig. 14).

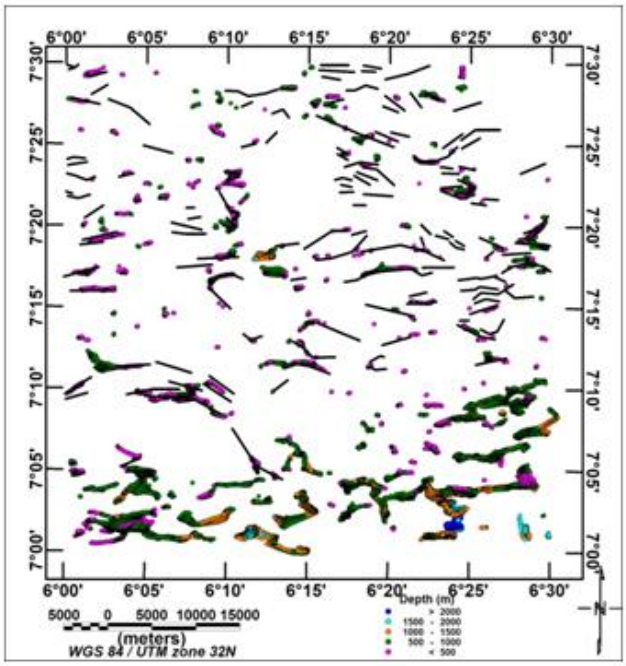

Fig. 13. Euler solutions (SI=1) with structures delineated from HGM (Map)

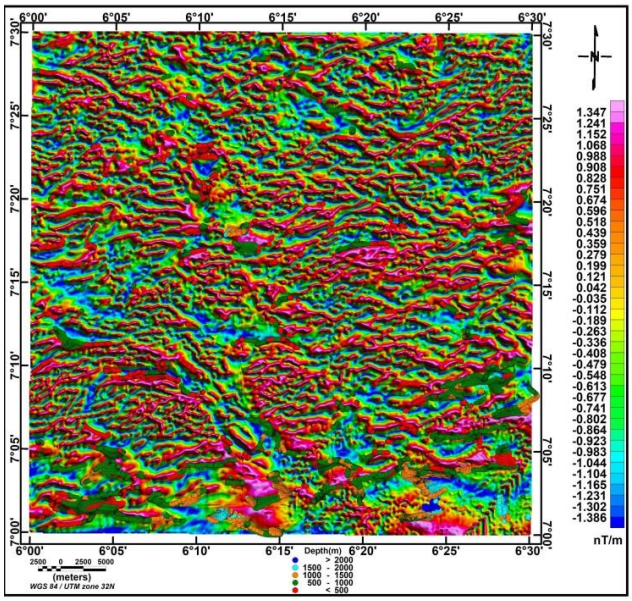

Fig. 14. TDR map with Euler solutions (SI=1)

4. CONCLUSION

The application of source edge mapping techniques such as Analytic signal (AS), Horizontal Gradient Magnitude (HGM), Tilt Derivative (TDR) has greatly contributed to the detection of anomaly source edge and delineation of geologic structures within the study area. It was observed that in structural delineation within the study area, the three approaches have complemented each other. The rocks within the study area, especially the basement rocks, have been affected by two tectonic trends which are predominant in the direction of ENE-WSW followed by WNW-ESE direction. Also, depth to magnetic source estimation using 3D Euler deconvolution and source parameter imaging (SPI) has shown that the two techniques also complement each other in-depth estimation and general depth to magnetic source was 50 m in the basement portion of the study area and >2000 m in sedimentary portion as obtained from both SPI and 3D Euler deconvolution techniques.

COMPETING INTERESTS

Authors have declared that no competing interests exist.

REFERENCES

1. Black R. Precambrian of West Africa. Episodes. 1980;4:3–8.
2. McCurry P. Pan-African Orogeny in Northern Nigeria. Geol. Soc. Am. Bull. 1971a;82,:3251-3262
3. Rahaman MA. Progressive polyphase metamorphism in pelitic schists around Aiyetoro, Oyo State, Nigeria. J. Min. Geol. 1976a;13:33- 44
4. Grant NK. Structural distinction between the metasedimentary cover and underlying basement in 600 M.Y. old Pan-African domain. Geol. Soc. Am. Bull. 1978;89:50-58.
5. Ekweme BN. Structural orientation and Precambrian deformational episode of Uwet area, Oban Massif, S. E. Nigeria. Precambrian Res. 1987;34:269-289.
6. Ekwueme BN. Structural features of Obudu Plateau, Bamenda Massif, Eastern Nigeria: Preliminary interpretation. J. Min. Geol. 1994;30(1):45-59.
7. Olasehinde PI, Awojobi, MO. Geologic and geophysical evidence of a North-South fracture system, East and West of the upper Gurarariver in Central Nigeria. Water Resources Journal. 2004;15(1):33-37
8. Oluyide PO. Structural trends in the Nigerian basement complex. Precambrian Geology of Nigeria, Geological Survey of Nigeria. 1988;93-98.
9. Udoh AN. Remote sensing imageries of Nigeria, north of 70401: In: Oluyide, P.O.et. al.,(eds). Precambrian Geology. Geological Survey of Nigeria, Publ. 1988;99-102.
10. Wright JB. Geology and mineral resources of West Africa. George Allen and Unwin, London. 1985;187.
11. NGSA. Geology and Structural Lineament Map of Nigeria; 2006.
12. Okpoli CC, Oludeyi D. Aeromagnetic Mapping of Iwo Region of Southwestern Nigeria of Lithostructural Delineation. Pakistan Journal of Geology. DOI: https://doi.org/10.2478/pjg-2019-0008
13. Olomo KO, Olayanju GM, Adiat KAN, Akinlalu AA. Integrated Approach Involving Aeromagnetic And Landsat For Delineating Structures And Its Implication On Mineralisation. International Journal of Scientific and Technology Research; 2018. ISSN 2277-8616.
14. Ayanwola MD, Bamisaiye OA. Geological Mapping of Igbara-Oke and Owena Area South Western, Nigeria. Iimatol Weather Forecasting. 2018;6:243. DOI:10.4172/2332-2594.1000243
15. Alabi AA, Olowofela O. Estimation of Source Parameters in Ibadan, South-Western Nigeria Using Digitized Aeromagnetic Data. Journal of Natural Science, Engineering and Technology; 2015. ISSN: Print - 2277 – 0593 Online - 2315 - 7461
16. Jayeoba A, Odumade D. Geological and Structural Interpretation of Ado-Ekiti Southwest and its Adjoining Areas Using Aeromagnetic Data. Adapted from extended abstract prepared in conjunction with the oral presentation given at Pacific Section AAPG, SEG and SEPM Joint Technical Conference, Oxnard, California; 2015. AAPG
17. Sunmonu LA, Olasunkanmi NK, Alagbe OA. Aeromagnetic data interpretation for geo-structural analysis of Ibadan, Southwestern Nigeria. International Journal of Engineering Research & Technology (IJERT). 2013;2(10). ISSN: 2278-0181

18. Storey BC. The role of mantle plumes in continental breakup: a case history from Gondwanaland, Nature. 1995;377:301-308.
19. Omatsola ME, Adegoke OS. Tectonic evolution and Cretaceous stratigraphy of the Dahomey basin; Journal of Mining and Geology. 1981;18(1):130-137.
20. Adediran SA, Adegoke OS. Evolution of the sedimentary basins of the Gulf of Guinea- Current Research in Africa Earth Sciences, Matheis and Schandeimeier (eds); Balkema, Rotterdam. 1987;283-286
21. Coker SJL, Ejedawe JE. Petroleum prospects of the Benin basin, Nigeria, Nig. Jour. of Min. and Geol. 1987;34:424-439.
22. Whiteman AJ. Nigeria: Its Petroleum Geology, Resources and Potential, vol.1&2, Graham and Trottan, London. 1982;:394.
23. Rajaram M. What's new in the interpretation of magnetic data? Geohorizons. 2009;50.
24. Salem A, Williams S, Fairhead JD, Smith R, Ravat DJ. Interpretation of magnetic data using tilt-angl derivatives. Geophysics. 2008;73: L1–L10.
25. Verduzco B, Fairhead JD, Green CM, MacKenzie C. The meter reader – new insights into magnetic derivatives for structural mapping. The Leading Edge. 2004;23:116–119.
26. Miller HG, Singh V. Potential field tilt – A new concept for the location of potential field sources. Journal of Applied Geophysics. 1994;32:213–217.
27. Roest W, Verhoef J, Pilkington M. Magnetic interpretation using 3-D analytic signal. Geophysics. 1992;57:116-125.
28. Hogg S. GT-Gradient tensor gridding, geologic structure, example, 2004. Available:http://www.shageophysics.com/
29. Phillips JD. Locating magnetic contacts; A comparison of the horizontal gradient, Analytic Signal and Local Wavenumber Methods: Society of Exploration Geophysicists, Abstracts with Programs, Calgary. 2000;402–405.
30. Grauch VSJ, Cordell L. Limitations of determining density or magnetic boundaries from the horizontal gradient of gravity or pseudo gravity data. Short note, Geophysics. 1987;52(1):118–121.
31. Reid AB, Allsop JM, Granser H, Millet AJ, Somerton IW. Magnetic interpretation in three dimensions using Euler deconvolution. Geophysics. 1990;55:80-91
32. Thompson DT. EULDPH: a new technique for making computer-assisted depth estimates from magnetic data. Geophysics. 1982;(47):31–37.
33. Salako KA. Depth to Basement Determination Using Source Parameter Imaging (SPI) of Aeromagnetic Data: An Application to Upper Benue Trough and Borno Basin, Northeast, Nigeria. Academic Research International. 2014;5(3). ISSN: 2223-9944, eISSN: 2223-9553
34. Thurston JB, Smith RS, Guillon JC. A multi-model method for depth estimation from magnetic data. Geophysics. 200;67(2):555–561
35. Thurston JB, Smith RS. Automatic conversion of magnetic data to depth, dip, and susceptibility contrast using the SPI method. Geophysics. 1997;62(3):807–813.
36. Thurston J, Guillon JC, Smith R. Model-independent depth estimation with the SPITM method: 69thAnnual International Meeting, SEG, Expanded Abstracts. 1999;403–406.
37. Lou Y, Xue D-J, Wang M. Reduction to the pole at the geomagnetic equator. Chinese Journal of Geophysics. 2010;53(6):1082-1089.
38. Li X. Magnetic reduction-to-the-pole at low latitudes; 2008.
39. Yaoguo L, Douglas WO. Stable reduction to the pole at the magnetic equator Geophysics. 2001;66(2):571–578.
40. Milligan PR, Gunn PJ. Enhancement and presentation of airborne geophysical data. AGSO Journal of Australian Geology and Geophysics. 1997;17(2):64–774.
41. Baranov V. A new method of interpretation of aeromagnetic maps: Pseudogravimetric anomalies. Geophysics. 1957;(22):259-283.
42. Telford WM, Geldart LP, Sherriff RE, Keys DA. Applied geophysics. Cambridge: Cambridge University Press. 1990;860.
43. Reynolds JM. An introduction to applied and environmental geophysics, John Wiley and Ltd. Bans Lane, Chichester. 1997;124-13.
44. Blakely RJ. Potential theory in gravity & magnetic applications, Cambridge University Press, Cambridge. 1995;1–437.
45. Phillips JD. Processing and Interpretation of Aeromagnetic Data for the Santa Cruz Basin – Patahonia Mountains Area, South-Central Arizona. US. Geological Survey Open-File Report, Arizona. 1998;02-98.

46. Salem A, Williams S, Fairhead JD, Smith R, Ravat DJ. Interpretation of magnetic data using tilt-angle derivatives. Geophysics. 2008;73:L1–L10.
47. Stavrev P, Reid A. Degrees of homogeneity of potential fields and structural indices of Euler deconvolution. Geophysics. 2007;72:L1-L12
48. Smith RS, Thurston JB, Dai TF, MacLeod. IN iSPI —- the improved source parameter imaging method: Geophysical Prospecting. 1998;46:141–151.
49. Tawey MD, Alhassan DU, Adetona AA, Salako KA, Rafiu AA, Udensi EE. Application of aeromagnetic data to assess the structures and solid mineral potentials in part of North Central Nigeria. Journal of Geography, Environment and Earth Science International. 2020;24(5):11-29. Article no.JGEESI.58030 ISSN: 2454-7352

Peer-review history:
The peer review history for this paper can be accessed here:
http://www.sdiarticle4.com/review-history/61526